Received: 24 August 2023 | Revised: 05 October 2023 | Accepted: 08 October 2023
DOI: 10.48309/jmpcr.2023.417750.1007
Journal of Medicinal and Pharmaceutical Chemistry Research
SAMI

FULL PAPER

Advancements in plasma-enhanced chemical vapor deposition of a multi-walled carbon nanotubes on Si/SiO_2 substrates: A comprehensive review

Rahadian Zainul[a,*] | Matlal Fajri Alif[b] | Ani Mulyasuryani[c]

[a]*Department of Chemistry, Faculty of Mathematics and Natural Sciences, Universitas Negeri Padang, Padang, West Sumatra, Indonesia*

[b]*Department of Chemistry, Faculty of Mathematics and Natural Sciences, Andalas University, Padang, West Sumatra, Indonesia*

[c]*Analytical Chemistry Laboratory, Department of Chemistry, Faculty of Mathematics and Natural Sciences, Universitas Brawijaya, East Java, Indonesia*

Corresponding Author:
Rahadian Zainul
E-mail: rahadianzmsiphd@fmipa.unp.ac.id
Tel.: +62 812-6138-53

This review study offers a thorough investigation of the developments in the field of multi-walled carbon nanotubes (MWCNTs) deposition on Si/SiO_2 substrates using plasma-enhanced chemical vapor deposition (PECVD). Using iron catalytic nanoparticles produced by the breakdown of Fe(CO)5, the study examines the growth mechanism of MWCNTs. According to prior literature descriptions, iron oxide nanoparticles are deposited using a microwave plasma torch with a dual-flow nozzle electrode. The Si/SiO_2 substrate is set up in a sample holder that can store several samples, each of which has a deposition area of 4 mm by 4 mm. Argon acts as the carrier gas and flows at preset rates via the inner and outer channels. At 210 W of plasma power, the deposition process lasts for 15 seconds. The resulting MWCNTs' structural characteristics, such as density, alignment, and uniformity, are examined. This comprehensive review highlights the intricate interplay of process parameters and their influence on MWCNT growth. The insights provided contribute to a better understanding of PECVD-based MWCNT synthesis and pave the way for optimizing these processes for various applications, including electronic and energy devices.

KEYWORDS

Plasma-enhanced chemical vapor deposition; multi-walled carbon nanotubes; Si/SiO_2 substrate; nanoparticle catalysis; growth mechanism.

Introduction

Due to its potential uses in numerous domains, the deposition of multi-walled carbon nanotubes (MWCNTs) onto Si/SiO_2 substrates using plasma-enhanced chemical vapor deposition (PECVD) has attracted a lot of attention. MWCNTs possess exceptional mechanical, electrical, and thermal properties that make them promising candidates for advanced electronic devices, sensors, and energy storage systems [1-3].

The PECVD technique offers precise control over the growth process and structural characteristics of MWCNTs, which is essential for tailoring their properties to specific applications. However, despite considerable progress, there remains a need to further understand the intricate interplay between process parameters, substrate properties, and

catalyst materials to achieve uniform and well-aligned MWCNTs with optimal properties. This review aims to bridge the gap in the existing knowledge by comprehensively analyzing the recent advancements in PECVD-based MWCNT deposition on Si/SiO_2 substrates, focusing on the growth mechanisms, catalyst nanoparticle formation, and the influence of deposition conditions on the resulting MWCNT structures [4-6].

Recent advancements in the field of multi-walled carbon nanotube (MWCNT) deposition on Si/SiO_2 substrates using plasma-enhanced chemical vapor deposition (PECVD) have underlined the importance of exact control over growth parameters and substrate interactions.. Advanced techniques for catalyst nanoparticle formation, such as the use of iron oxide nanoparticles derived from $Fe(CO)_5$ decomposition, have demonstrated improved control over MWCNT growth. Moreover, strategies to enhance uniformity and alignment of MWCNTs through improved carrier gas flow control, substrate preparation, and optimized plasma power have been explored [7-8].

The characterization of resulting MWCNT structures, including density, alignment, and uniformity, has been a focal point of recent research, leading to valuable insights into tailoring MWCNT properties for specific applications. The integration of MWCNTs into electronic devices, sensors, and energy storage systems remains a driving force, emphasizing the need for continued advancements in PECVD techniques to meet the demands of emerging technologies. This state-of-the-art understanding underscores the importance of exploring novel catalyst materials, optimizing deposition conditions, and gaining insights into the growth mechanisms of MWCNTs on Si/SiO_2 substrates [9-11].

The originality of this study is found in its thorough investigation of plasma-enhanced chemical vapor deposition (PECVD) methods for the precise deposition of multi-walled carbon nanotubes (MWCNTs) on Si/SiO_2 substrates. By focusing on the intricate interplay between process parameters, substrate properties, and catalyst materials, this study contributes to an improved understanding of the growth mechanisms and structural characteristics of MWCNTs. [12-13]

Additionally, the utilization of iron oxide nanoparticles as catalysts, derived from $Fe(CO)_5$ decomposition, offers a novel approach to enhance MWCNT growth control. The optimization of carrier gas flow rates, substrate preparation, and plasma power allows for the production of uniform and aligned MWCNT structures, which are crucial for various applications. The ultimate goal of this research is to advance the knowledge and techniques related to PECVD-based MWCNT deposition, facilitating their integration into electronic devices, sensors, and energy storage systems with tailored properties and enhanced performance [14-15].

Martials and methods

Materials

Several important diagnostic devices were utilized to analyze and comprehend the characteristics of multi-walled carbon nanotubes deposited. Examples of device types include high-resolution SEM, such as the Hitachi S-4800 SEM model, enabling detailed surface imaging and nanotube morphology examination. Furthermore, XRD with the Rigaku SmartLab XRD model was employed for crystallographic analysis and understanding the crystal structure of nanotubes. Meanwhile, Raman spectroscopy with the Horiba LabRAM HR Evolution Raman Spectrometer allowed for in-depth molecular vibration analysis. Lastly, FT-IR with the Thermo Scientific Nicolet iS50 FT-IR Spectrometer was used for infrared analysis, aiding in the characterization of chemical composition and molecular bonds on the carbon nanotube's surface. All of these devices

represent cutting-edge technology that provides profound insights into the advancements in Plasma-Enhanced Chemical Vapor Deposition and the properties of nanomaterials deposited on Si/SiO_2 substrates.

Preparation of substrates and nanoparticle deposition

Si/SiO_2 substrates were meticulously prepared to ensure cleanliness and uniformity. The substrates were then placed within a specialized holder designed to accommodate up to four samples simultaneously. A microwave plasma torch with a dual-flow nozzle electrode was used to deposit iron oxide nanoparticles onto the substrates, which are necessary for starting the formation of multi-walled carbon nanotubes (MWCNTs). [16-17]. This methodology allowed for controlled nanoparticle formation through the decomposition of $Fe(CO)_5$. The choice of argon gas as the carrier gas was based on its inert nature, preventing undesirable reactions during nanoparticle deposition. Flow rates of 700 and 28 sccm were respectively maintained through the central and outer channels, with the outer channel facilitating the introduction of $Fe(CO)_5$ vapors [18-19].

Standart and procedur

Deposition of Multi-Walled Carbon Nanotubes (MWCNT) Using Plasma-Enhanced Chemical Vapor Deposition. MWCNTs were deposited on Si/SiO_2 substrates using the plasma-enhanced chemical vapor deposition method. To avoid contamination, the prepared substrates were loaded into a chamber with a controlled atmosphere. Ethyl carbonate and propylene carbonate (EC:PC, 9:1, v/v) were added to the process as the electrolyte, along with 1.0 mol L1 NaPF6. The mixture was introduced into the chamber and underwent the process under controlled conditions. The plasma power, deposition time, and gas flow rates were maintained at 210 W, 15 seconds, 700 sccm for the central channel, and 28 sccm for the outer channel, respectively. This established protocol enabled the controlled growth of MWCNTs on the iron oxide nanoparticles [20-21].

To assess the density, alignment, and homogeneity of the synthesized MWCNTs, extensive structural characterisation was performed on them. The morphological properties of the produced MWCNTs were observed using scanning electron microscopy (SEM), allowing evaluation of their alignment and distribution. The MWCNTs' vibrational characteristics were examined using Raman spectroscopy to gain knowledge of their structural integrity and caliber. The results obtained from these characterization techniques were interpreted to understand the effects of varying deposition parameters on the final MWCNT structures [22-23].

Results and discussion

Controlled Growth of MWCNTs. The research's primary focus on the controlled deposition of multi-walled carbon nanotubes (MWCNTs) on Si/SiO_2 substrates through plasma-enhanced chemical vapor deposition (PECVD) highlights its significance for tailored nanomaterial synthesis. The utilization of iron oxide nanoparticles as catalysts, derived from $Fe(CO)_5$ decomposition, presents a novel approach to enhance MWCNT growth control. The optimized carrier gas flow rates, substrate preparation, and plasma power contribute to the production of uniform and aligned MWCNT structures, which are pivotal for numerous applications in electronics and energy storage systems.

Structural characterization insights

The integration of scanning electron microscopy (SEM) and Raman spectroscopy for structural characterization provided

comprehensive insights into the synthesized MWCNTs. SEM images allowed the assessment of the MWCNT alignment, density, and distribution, enhancing the understanding of their morphology. Additionally, Raman spectroscopy data enabled the analysis of vibrational spectra, revealing details about the crystalline structure, quality, and potential defects in the grown MWCNTs. These analyses facilitated the establishment of correlations between deposition parameters and structural attributes, enabling the identification of optimal conditions for controlled MWCNT growth [24-26].

The findings of this research hold significant implications for various nanomaterial applications. Controlled MWCNT growth techniques are essential for tailoring the properties of nanomaterials to meet specific requirements in electronic devices, sensors, and energy storage systems. The exploration of advanced catalys materials and optimized deposition conditions opens avenues for enhancing the performance of these applications. Moreover, the comprehensive analysis of the relationships between deposition parameters and MWCNT structural attributes contributes to a better understanding of plasma-enhanced chemical vapor deposition processes, facilitating their utilization in various emerging technologies [27-29].

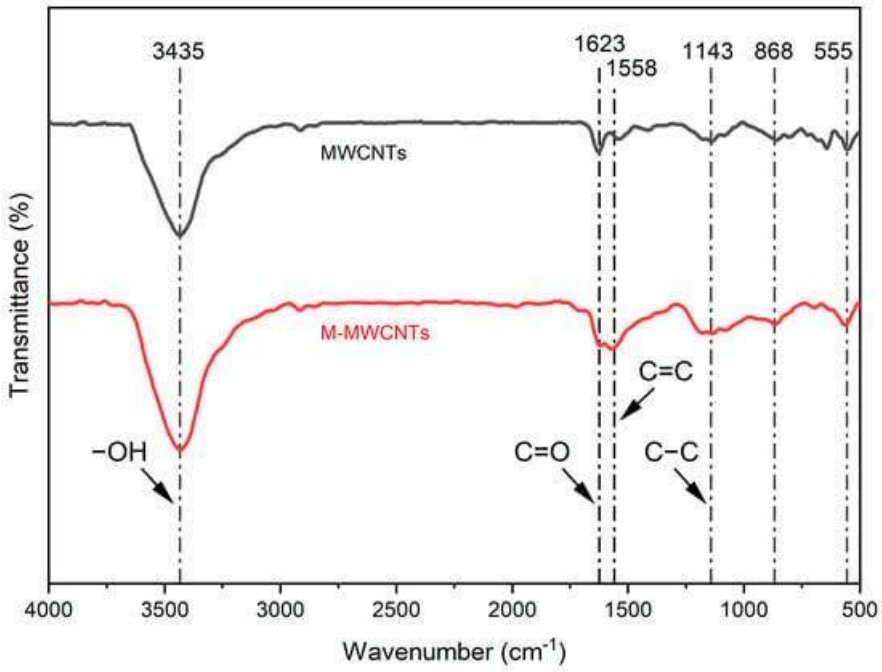

FIGURE 1 MWCNTs and M-MWCNTs' FTIR spectrum

The structural examination of MWCNTs and M-MWCNTs was affirmed through FT-IR analysis, with subsequent oxidation and acidification modifications applied to M-MWCNTs. Figure 1 depicts the FTIR spectra, revealing the presence of functional groups on both the interior and exterior surfaces of MWCNTs and M-MWCNTs. These functional groups include OH groups (3200–3600 cm^{-1}), C=O groups (1600 cm^{-1}), and C–C groups (1150 cm^{-1}). In comparison to the original MWCNTs, M-MWCNTs exhibited increased transmittance (%) for the OH and C=O groups due to the modification process, which augmented the number of active sites and consequently altered the surface polarity and charge distribution. It is worth noting that the stretching vibration absorption peak of C=O

typically falls within the range of 1755–1670 cm^{-1}. In this study, a C=O absorption peak was observed at 1623 cm^{-1}. This shift to a shorter wavelength region is attributed to the conjugate effect of carbon nanotubes, a phenomenon observed in prior research as well [30,31].

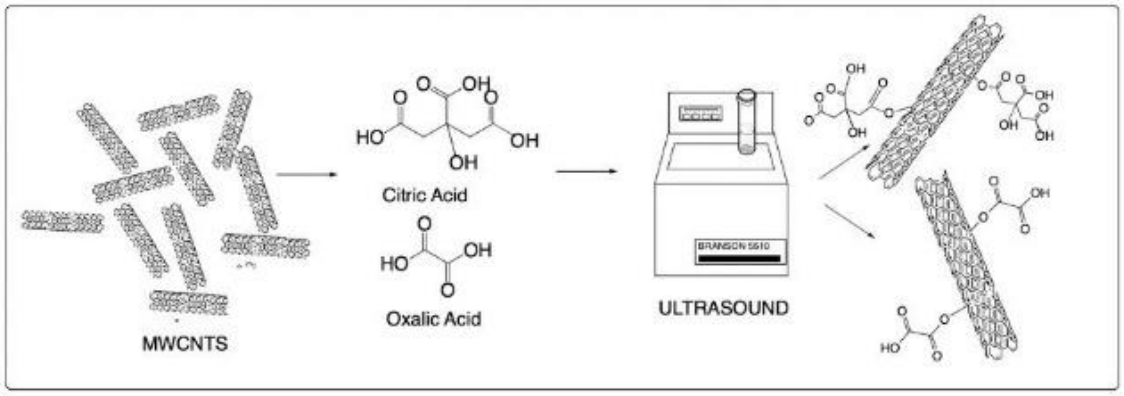

FIGURE 2 Multiple-wall carbon nanotube (MWCNT) modification using ultrasound and oxalic and citric acids

Test tubes containing 200 mg of MWCNTs were mixed with saturated aqueous solutions of organic acids, namely citric acid and oxalic acid, as shown in Figure 2. It's important to note that each acid exhibits different solubility characteristics, and the solutions used in this study were intentionally prepared to be saturated. Consequently, the solubility of these acids varied depending on factors like concentration and temperature, affecting the amount of citric acid and oxalic acid dissolved in the water. Citric acid was introduced in a 1:1 ratio, while oxalic acid was used in a 1:0.5 ratio in relation to the MWCNTs. After the MWCNTs were combined with the saturated acid solutions, they underwent a sonication process for 180 minutes at a temperature of 40 °C. An ultrasound bath from BRANSON, located in Brookfield, CT, USA, was utilized for this purpose. Following sonication, the MWCNT-acid mixtures were filtered and subsequently subjected to vacuum drying for a duration of 24 hours at a temperature of 50 °C. [32-33].

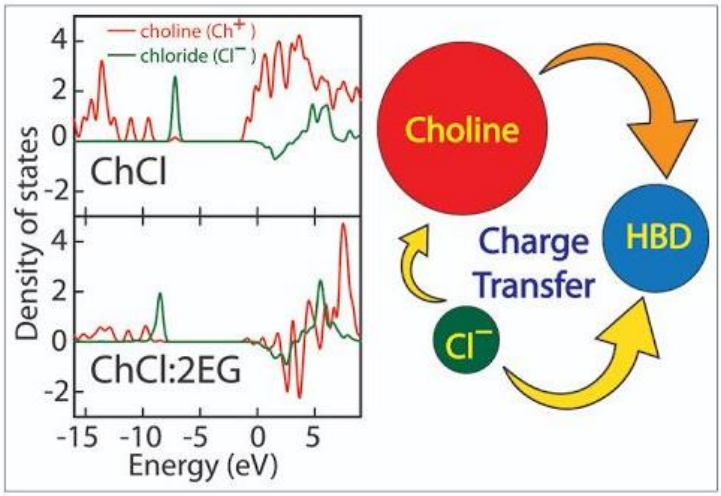

FIGURE 3 Three well-known deep eutectic solvents

We present the outcomes of quantum chemical computations concerning three widely recognized deep eutectic solvents (DESs), as shown in Figure 3. Our goal is to elucidate the molecular interactions, charge transfer phenomena, and thermodynamic properties within these systems. The three DESs subject to our investigation include the 1:1 mixture of choline chloride and malonic acid, referred to as "maloline," the 1:2 blend of choline chloride and ethylene glycol, known as "reline," and the 1:2 combination of choline chloride and urea, termed "ethaline."

To identify the predominant interactions within these DES systems, we leveraged the strong correlation between the vibrational spectra computed through our calculations and those observed experimentally. Our findings revealed that these DESs are stabilized by a combination of conventional hydrogen bonds and interactions occurring between their individual components (specifically, C-H•••O and C-H••• interactions). It's noteworthy that the hydrogen-bonding network in the original hydrogen-bond donor dimer differs significantly from the one established in the DES [34-36].

An examination of the density of states reinforces the direction of charge transfer within these systems. Moreover, the charge decomposition analysis indicates a notable transfer of charge from choline and chloride ions to the hydrogen-bond donor, with a more substantial contribution coming from the cation (choline). Consequently, there exists a correlation between the bond orders of the choline-chloride interactions in deep eutectic solvents (DESs) and their respective melting points. This correlation sheds light on how the adjustment of hydrogen-bond donors influences the strength of choline-chloride interactions, which in turn impacts the physical properties of DESs.

Lastly, the observed variations in vibrational entropy changes align with the general trend in entropy changes that occur upon the formation of DESs [37-39].

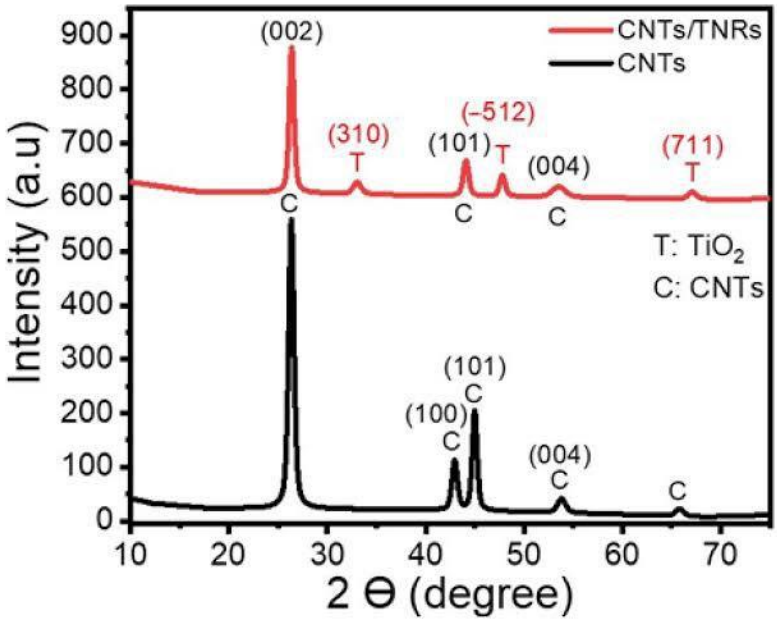

FIGURE 4 The TNR/CNT nanocomposite was examined using XRD spectroscopy to determine its crystal structure

Figure 4 presents XRD charts for both the nanocomposite CNTs and TNRs/CNTs. In the CNTs chart, a noticeable peak corresponding to XRD diffraction from the (002) plane is

observed at an angle of 26.32°. Additional reflections related to carbon's in-plane (100) and (101) positions are evident in the peaks at 42.91° and 44.94°, respectively. The peak at 65.74° is associated with XRD from the (004) plane.

In the XRD pattern of TNRs/CNTs, three distinct peaks are visible at angles of 2θ = 26.34°, 44.05°, and 53.48°, corresponding to the (002), (101), and (004) planes, respectively. Furthermore, the chart displays peaks at 33.0°, 47.76°, and 67.02°, which are attributed to the (310), (512), and (711) planes and are indicative of TiO_2-B. [40,41].

The Scherrer equation, given by CS = 0.9 * λ / (cosθ), where λ is the X-ray wavelength (for example, CuKα = 0.15405 nm), θ is the Bragg's angle in radians, and CS is the average crystallite size, was employed to compute the average crystallite size (CS).

To determine the dislocation density (ρ), Williamson and Smallman's formula was used, where N = 1 signifies the minimum dislocation density, and ρ = N * CS^(-2).

The texture coefficient (TC) is calculated using Equation (1). However, the specific details of Equation (1) are not provided in your text, so you would need to refer to the actual equation or provide it for a more detailed explanation.) [42,43].

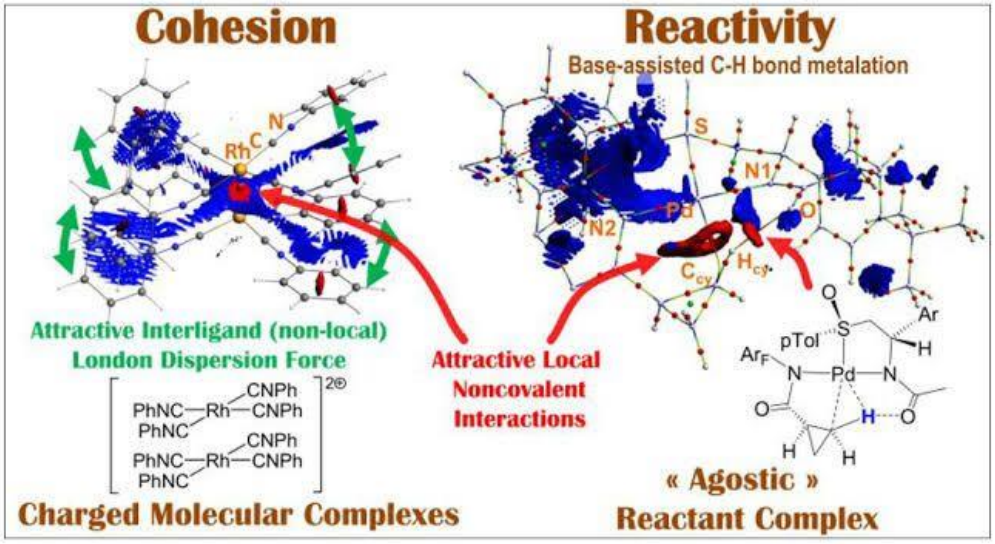

FIGURE 5 NCIs (noncovalent interactions)

A substantial community of chemists has dedicated significant efforts to the study of noncovalent interactions (NCIs) over an extended period, as shown in Figure 5. Their research has explored what are often referred to as the "canonical categories" of NCIs, which have been derived from descriptive crystallography. These categories encompass a range of interactions, including hydrogen bonds, π-interactions, halogen/chalcogen/tetrel bonds, cation-π interactions, C-H interactions, metallophilic interactions in a broad sense, and more.

Recent advancements in theoretical chemistry have introduced innovative approaches for investigating noncovalent interactions. Notably, dispersion-force-inclusive density functionals have emerged as reliable tools for modeling systems ranging from small molecules to large molecular complexes. These functionals provide a comprehensive framework for considering

dispersion forces, which are critical components of NCIs.

Two prominent computational methods, DFT-D (Density Functional Theory with Dispersion Correction) and ab initio calculations, are employed to analyze the contributions of London, Debye, and Keesom forces. These forces represent the three primary types of van der Waals interactions. Importantly, these methods enable a detailed examination of these forces while maintaining computational efficiency, making them valuable tools for understanding the intricacies of noncovalent interactions [44-46].

Over the past 15 years, our research has been dedicated to exploring the role of noncovalent interactions (NCIs) in the cohesion of organometallic complexes. We've investigated how NCIs operate within both the primary and secondary coordination spheres of the metal, as defined by Werner's coordination theory.

Our studies have revealed that NCIs play a crucial role in various aspects of organometallic chemistry. Specifically, we have observed their significance in metal-metal donor-acceptor complexes, the self-aggregation of cationic Rh(I) chromophores, and the stabilization of electron-unsaturated transition metal complexes through hemichelation. In all of these cases, the London dispersion force has emerged as a critical attractive force that operates across the entire molecule or molecular assembly, contributing to the overall stability and behavior of these organometallic systems [47-49]

While we have made significant progress in our ability to analyze bonding and molecular cohesion in transition-metal-based organometallic systems, a larger question remains: can contemporary theoretical methods guide us in exploring reactivity and engineering novel catalytic systems? This question is at the heart of our research efforts, particularly in the realm of reaction and catalyst engineering.

To address this question, we focused on the study of transition metal-catalyzed directed C-H bond functionalization. This process involves the activation of ambiphilic metal-ligand interactions and concerted metalation-deprotonation steps. Our project was initiated with the goal of establishing a rationale for transitioning from the use of 4th and 5th row transition metals to more readily available 3rd row metals, thus promoting the use of earth-abundant elements in catalysis. This research seeks to not only understand the fundamental aspects of these reactions but also to enable the development of more sustainable and environmentally friendly catalytic systems [50-52].

In the base-assisted method of C-H bond metalation, agonistic interactions are indeed essential, but they alone are not enough to facilitate the process effectively. What truly enables the dissolution of C-H bonds in this context is a combination of factors. One crucial aspect involves minimizing the repulsion between the metal and the hydrogen atom (metal-H repulsion), while another pivotal factor is the favorable noncovalent interaction (NCI) coding associated with a proton-transfer step.

This Account outlines how our research focus has recently evolved towards the development of a chemical reactivity engineering paradigm that incorporates NCI effects as a fundamental consideration. To achieve this, we leverage state-of-the-art theoretical tools and experimental investigations. By integrating these approaches, we aim to gain a comprehensive understanding of the underlying principles that govern reactivity in chemical processes, ultimately leading to the development of more efficient and innovative chemical transformations. [53,54].

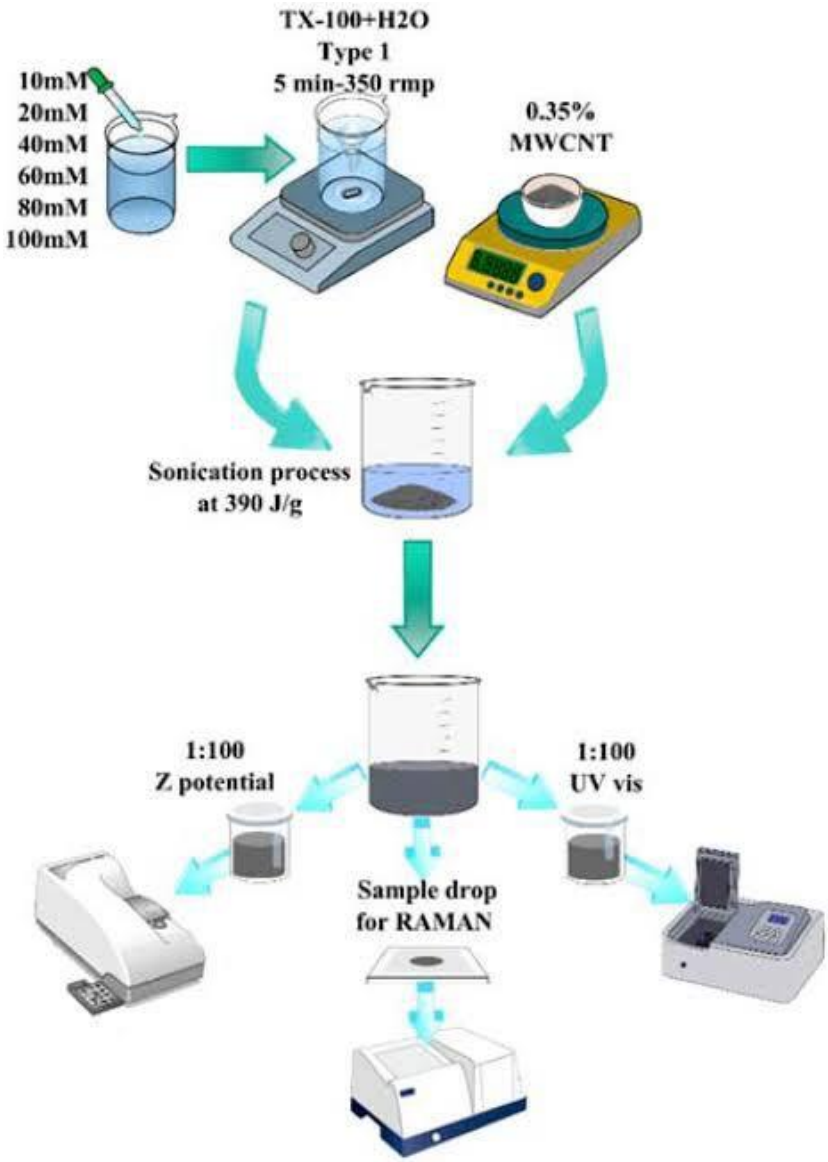

FIGURE 6 The process flow diagram for making and evaluating MWCNTs dissolved in type 1 water while adjusting the surfactant's molarity from 10 mM to 100 mM

Nanomaterials incorporated into cement pastes have garnered significant attention due to their wide-ranging applications, making them a vital area of research within the cement industry. This study is designed to investigate how changes in the molarity of dispersed multiple-wall carbon nanotubes (MWCNTs) and varying storage durations impact the mechanical properties of cement paste.

The investigation involved utilizing different surfactant molarities for the dispersion of 0.35% MWCNTs. Specifically, the following surfactant molarities were employed: (10, 20, 40, 60, 80, 20, 100) mM, as shown in Figure 6. This approach aims to shed light on the influence of MWCNT concentration and storage time on the mechanical characteristics of cement paste, providing valuable insights into their potential applications and performance in construction materials, as shown in Figure 7. [55-57].

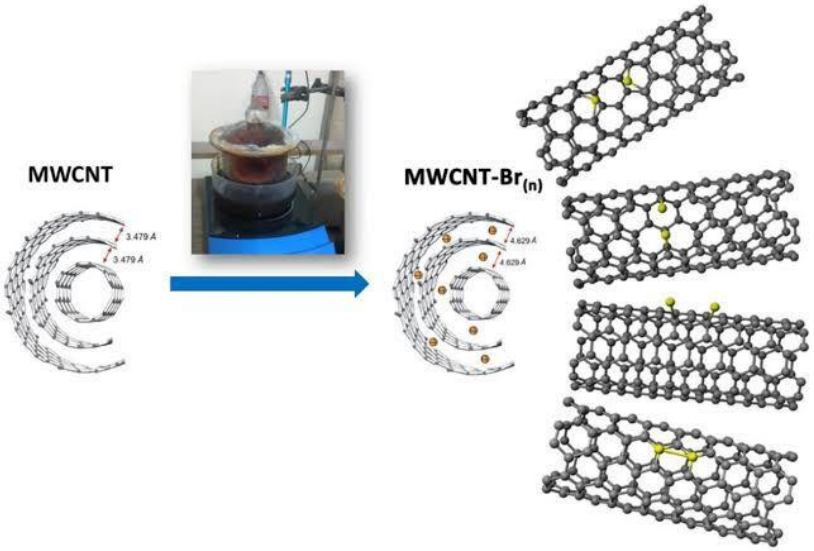

FIGURE 7 An illustration of the experimental setup

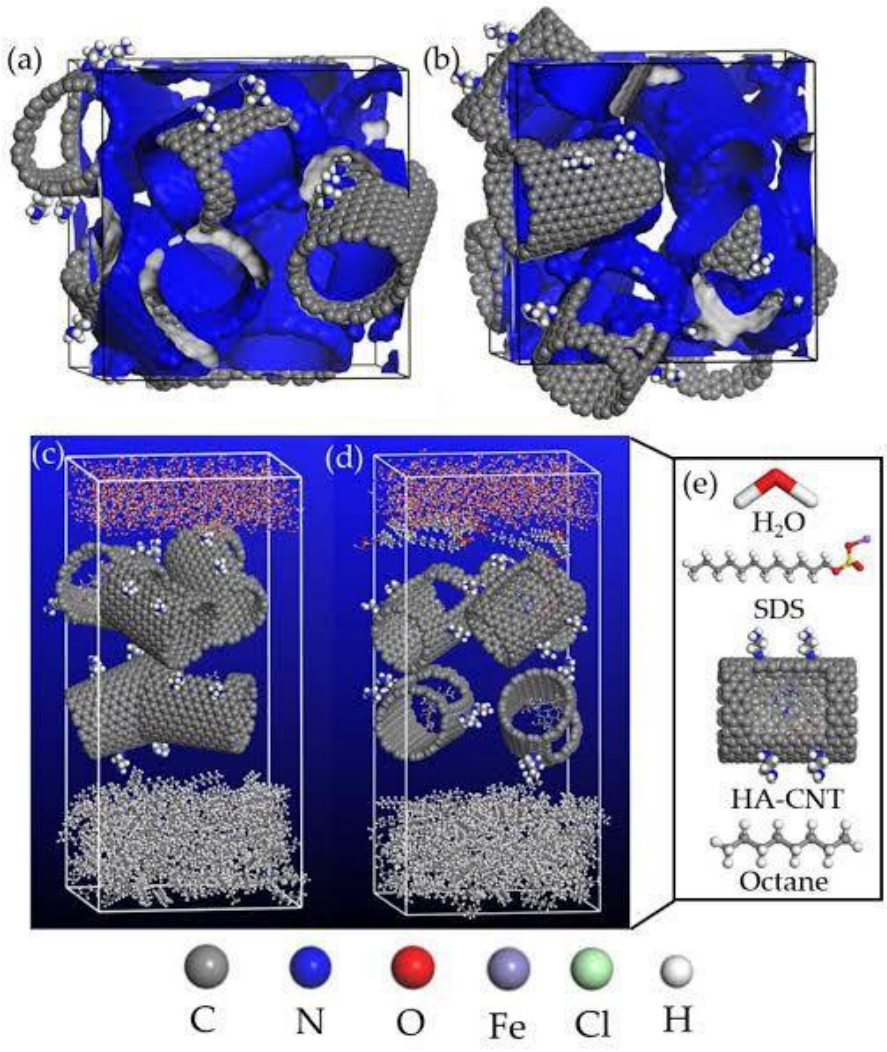

FIGURE 8 the seven units of the energy-minimized amorphous cells

Native MWCNTs (20 mg) were placed on a glass Petri dish, and a vessel containing liquid bromine (50 mL) was sealed over the plate. In order to raise the bromine vapor pressure in the tank, there were three cycles of 7, 10, and 14 days of intensive magnetic stirring. The vessel was heated to 30 °C while submerged in an oil bath. Following that time, the crude product was purified using the Drabowicz, Ciesielski, and Kulawik technique. To quickly and safely neutralize the bromine fumes, they were blasted out of the tank and into a sealed container containing sodium thiosulfate. They were then centrifuged at 14000 rpm until they reached a pH of neutral after being cleaned with distilled water. The remaining material was then centrifuged after being added methanol. The leftovers were heated at 65 °C in the oven for at least 12 hours. After adding 10 mL of benzene to the sample to bind unreacted bromine, it was centrifuged once more. The benzene was then decanted, and the residue was kept for at least 12 hours in an oven at 80 °C to dry [58-60].

The energy-minimized amorphous cells with seven units of the membrane active layer are shown in Figure 8. The free accessible volume within the membrane materials at a probe radius of 0.84 is shown by the blue and grey isosurfaces. For the NH2-CNT (Figure 8a) and the HA-MWCNT (Figure 8b), the Connolly surface areas were estimated to be 20,000 and 25,000 2, respectively. This significantly improves the accessibility of HA-MWCNT to solvents. In contrast, the Bondi equation's predicted fractional free volume (FFV) for the NH2-CNT and HA-MWCNT systems, respectively, yielded values of 0.296 and 0.305 that were consistent with the Connolly surface area [61,62].

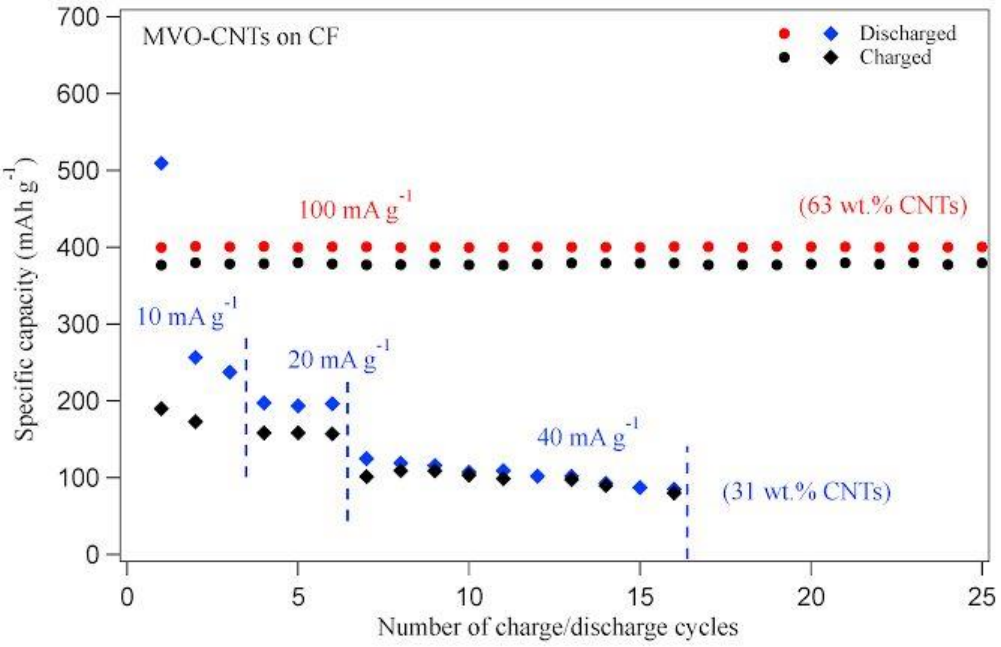

FIGURE 9 The MVO-CNTs' specific capacity as a function of galvanostatic charge/discharge cycles at various current density values

The electrochemical characterization was conducted within Swagelok-type cells, using a polypropylene membrane (designated as Celgard 2300) as the separator, and metallic sodium served as both the counter and reference electrode. To create the electrolyte, a solution was prepared by mixing 1.0 mol L-1 of NaPF6 with a blend of ethyl carbonate and propylene carbonate (EC:PC, 9:1, v/v 96 chameleon Reagent). Throughout this research, the MVO-CNTs/CF electrode underwent a series of 20 discharge/charge

cycles, ranging from 1.0 to 3.5 V vs. Na/Na+ at the gravimetric density as shown in Figure 9. In a similar manner to a previous study [26], which employed MVO-CNTs as a model for pseudo-capacitive behavior, two voltammetric cycles were executed at the same potential window scan rate of 0.5 mV.s. Prior to assembling the cells, the electrodes were subjected to thermal treatment for 12 hours at a temperature of 100°C and reduced pressure conditions. The assembly of the cells took place in a glove box filled with argon. [63-65].

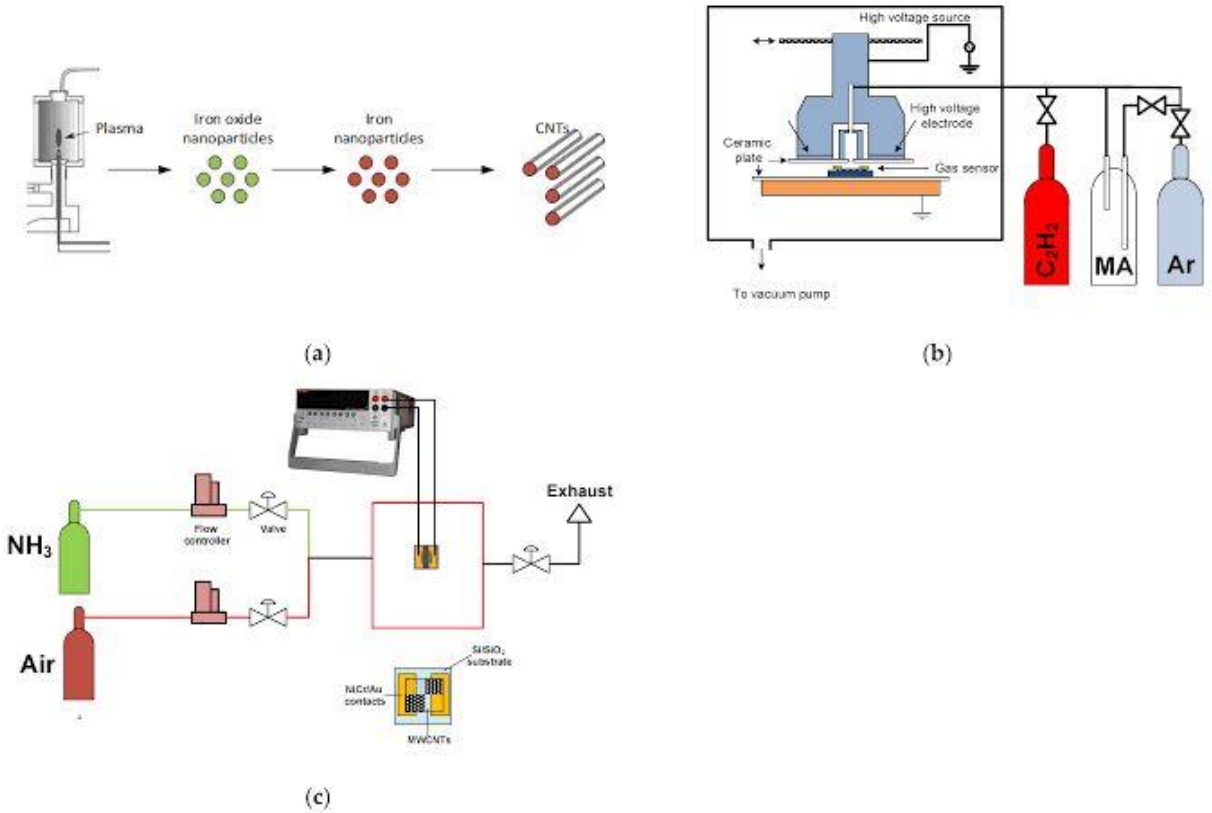

FIGURE 10 A diagram showing all the steps in the synthesis of MWCNTs

MWCNTs were synthesized on a Si/SiO_2 substrate using a plasma-enhanced chemical vapor deposition (PECVD) technique, as depicted in Figure 10a. The growth of carbon nanotubes (CNTs) occurred on iron catalytic nanoparticles, which were formed through the decomposition of Fe(CO)5.

To facilitate this process, a dual-flow nozzle electrode and a microwave plasma torch were utilized for depositing the iron oxide nanoparticles. Each sample featured a deposition area measuring 4 mm x 4 mm on a Si/SiO_2 substrate, with all samples arranged in a holder. Argon gas was employed as the carrier gas, with flow rates of 700 sccm and 28 sccm for the center and outer channels, respectively. The Fe(CO)5 vapor was introduced through the outer channel. The nanoparticle deposition was carried out for 15 seconds, employing 210 W of plasma power. [66,67].

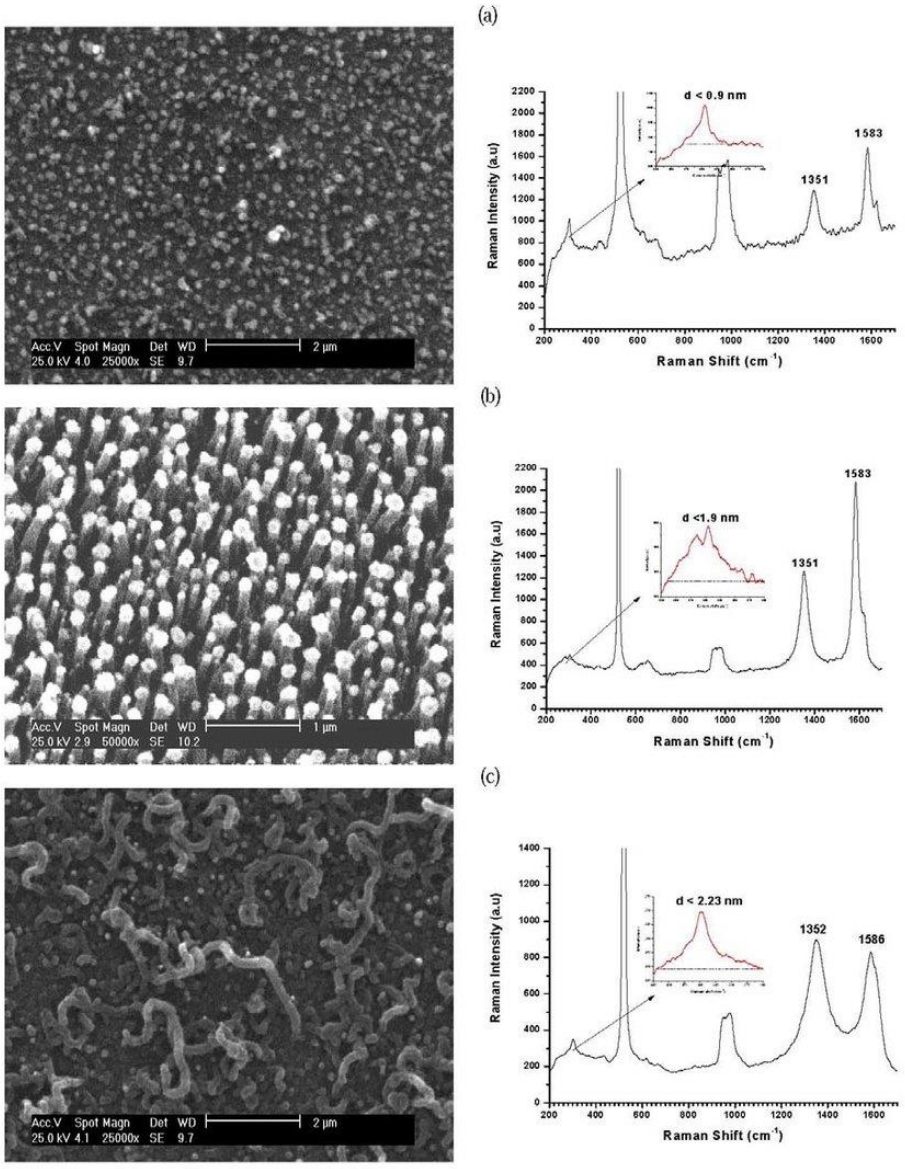

FIGURE 11 SEM images and corresponding Raman spectra were obtained from various samples prepared using an acetylene flow rate of 100 sccm and different plasma conditions, specifically, a) 20 mA, b) 50 mA, and c) 70 mA. The insets provide additional information, including the RBM (Radial Breathing Mode) frequencies and the corresponding diameters of the Single-Walled Carbon Nanotubes (SWNTs).

The provided description corresponds to an experimental setup involving Scanning Electron Microscope (SEM) imaging and Raman spectroscopy analysis of various samples. These samples were prepared under specific conditions, including an acetylene flow rate of 100 standard cubic centimeters per minute (sccm) and varying levels of plasma exposure at three different intensities: a) 20 mA, b) 50 mA, and c) 70 mA. The purpose of this investigation was to examine the structural and chemical properties of the samples under different plasma conditions [68].

In addition to SEM images and Raman spectra, the description mentions "insets" that provide additional information. Specifically, these insets offer insights into the Radial Breathing Mode (RBM) frequencies and the corresponding diameters of Single-Walled Carbon Nanotubes (SWNTs) present in the samples, as shown in Figure 11. This

comprehensive approach allows researchers to gain a better understanding of how different plasma conditions influence the growth and properties of SWNTs, as the RBM frequencies and diameters serve as crucial indicators of the nanotubes' structural characteristics.

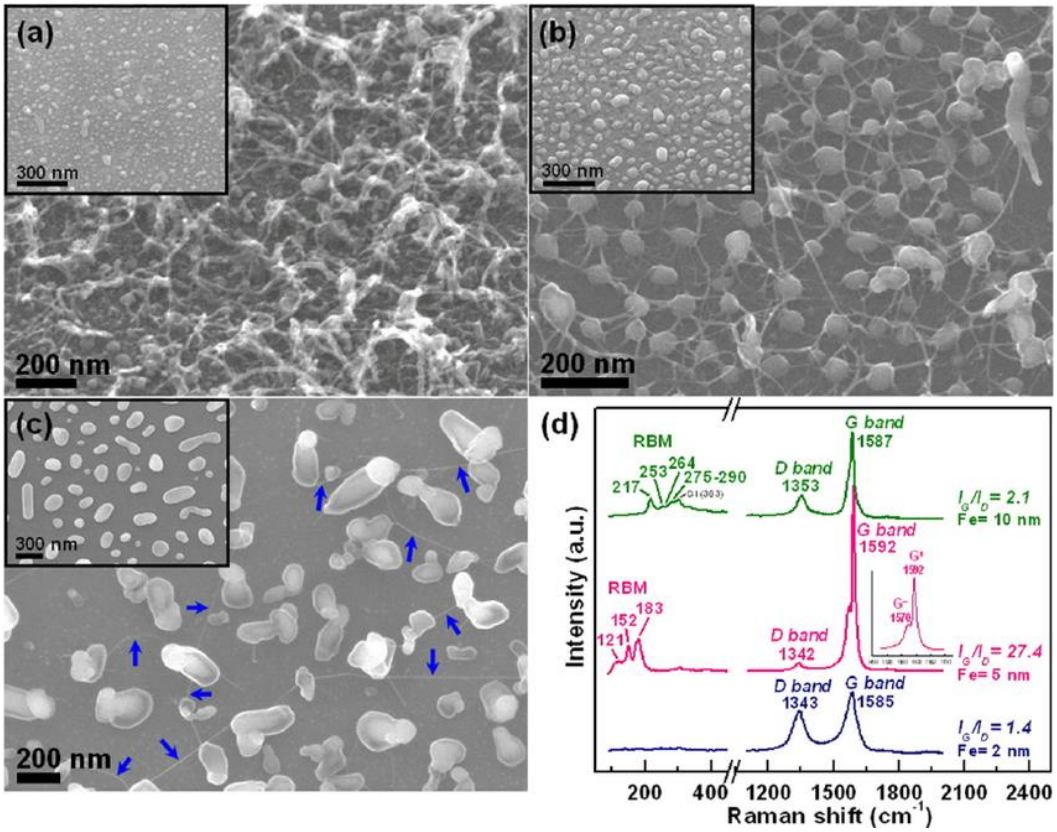

FIGURE 12 SEM images and Raman spectra were acquired for Carbon Nanotubes (CNTs) grown on $Al_2O_3/SiO_2/Si$ substrates with Fe precursor films of varying thickness, namely (a) 2 nm, (b) 5 nm, and (c) 10 nm. Additionally, (d) the corresponding Raman spectra were obtained. The insets in (a), (b), and (c) feature SEM images of the H-plasma-pretreated samples, prepared under specific conditions, including a CH_4/H_2 ratio of 1, a flow rate of 300 sccm, a working pressure of 16 Torr, and a plasma power of 750 W, with a growth time of 6 minutes.

The presented Figure 12 showcases a comprehensive analysis of Carbon Nanotubes (CNTs) grown on Al2O3/SiO_2/Si substrates, featuring Scanning Electron Microscope (SEM) images and Raman spectroscopy data. The study focuses on CNTs grown with Fe precursor films of varying thickness, specifically (a) 2 nm, (b) 5 nm, and (c) 10 nm. SEM images provide detailed visual insights into the morphological characteristics of these CNTs, highlighting how the thickness of the Fe precursor films influences their growth and structure. Additionally, (d) corresponding Raman spectra were collected, offering valuable information about the vibrational and structural properties of the CNTs under different film thickness conditions [69].

Moreover, the insets in (a), (b), and (c) offer SEM images of H-plasma-pretreated samples. These samples were prepared under specific conditions, which included a CH4/H2 ratio of 1, a flow rate of 300 sccm, a working pressure of 16 Torr, and a plasma power of 750 W, with a growth time of 6 minutes. These insets demonstrate the impact of plasma pretreatment on the CNTs' growth and morphology, providing a comprehensive understanding of how various parameters influence the development of CNTs on $Al_2O_3/SiO_2/Si$ substrates.

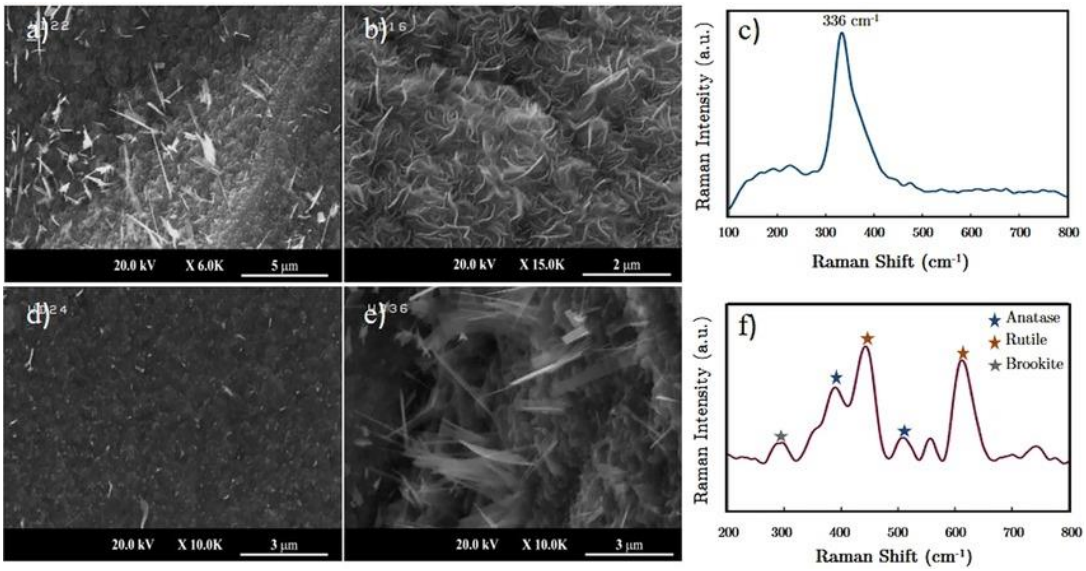

FIGURE 13 SEM images and their corresponding Raman spectroscopy results depict various structures grown on titanium substrates following a pre-cleaning process. (a) Shows the growth of TiO_2 nanowhiskers in an Ar-Ar/O_2 environment, while (b) displays the growth of TiS_2 nanosheets in an Ar/Cl_2 (2%)-Ar/O2 environment. (c) Features the Raman spectroscopy results for (b). (d) Represents a sample subjected to abrupt extraction using a cooling and venting apparatus following sulfurization. (e) Illustrates the transformation of 3D sheets in the growth environment of Ar/Cl_2 (0.5%)-Ar/O2 gas streams. Lastly, (f) presents the observed Raman spectroscopy results for (e), confirming the presence of Anatase, Rutile, and Brookite phases within the TiO_2 structures

The provided Figure 13 offers a comprehensive insight into a research study involving Scanning Electron Microscope (SEM) images and Raman spectroscopy results. It portrays the diverse range of structures cultivated on titanium substrates subsequent to a meticulous pre-cleaning process. In (a), the image highlights the successful growth of TiO_2 nanowhiskers in an Ar-Ar/O_2 environment. In (b), a contrasting scene emerges, showcasing the development of TiS2 nanosheets within an Ar/Cl_2 (2%)-Ar/O_2 environment. The ensuing (c) section exhibits the Raman spectroscopy outcomes for the TiS_2 nanosheets, offering valuable information regarding their structural properties and vibrational characteristics [70].

The visual narrative proceeds to (d), where we witness a sample that has undergone an abrupt extraction process through the utilization of a cooling and venting apparatus following sulfurization. This process is instrumental in altering the sample's morphology and properties, marking an important phase in the study. The subsequent sequence, featured in (e), portrays the transformation of 3D sheets within the growth environment of Ar/Cl_2 (0.5%)-Ar/O_2 gas streams, presenting another facet of the research's findings. Lastly, (f) delivers the observed Raman spectroscopy results for the transformed 3D sheets in (e), ultimately confirming the presence of Anatase, Rutile, and Brookite phases within the TiO_2 structures, thus shedding light on the structural diversity within the materials grown on the titanium substrates.

Conclusion

In conclusion, this research underscores the significance of plasma-enhanced chemical vapor deposition (PECVD) for the controlled

growth of multi-walled carbon nanotubes (MWCNTs) on Si/SiO_2 substrates. The utilization of iron oxide nanoparticles as catalysts introduces a novel approach to enhance growth uniformity and alignment, thereby enabling tailored nanotube structures. The comprehensive structural characterization, achieved through scanning electron microscopy (SEM) and Raman spectroscopy, provides in-depth insights into MWCNT properties and their correlation with deposition parameters. These findings hold promising implications for nanomaterial applications, positioning PECVD as a pivotal technique for advancing nanotechnology and facilitating the development of high-performance electronic devices and energy storage systems.

Acknowledgements

The author also thanks the technical and financial assistance from Riset Kolaborasi Indonesia, Scheme A for Fiscal Year 2023 with contract number 1500/UN35.25/LT/2023.

Conflict of Interest

The authors declare that there are no conflicts of interest regarding the publication of this paper. We confirm that this research was conducted impartially and without any external influence. We would like to express our gratitude to all individuals and organizations involved in this research for their support and collaboration, without which this study would not have been possible.

Orcid:

Rahadian Zainul:
https://www.orcid.org/0000-0002-3740-3597
Matlal Fajri Alif:
https://www.orcid.org/0000-0003-2718-6880
Ani Mulyasuryani:
https://www.orcid.org/0000-0001-9984-0007

References

[1] M.R. Baez-Gaxiola, J.A. García-Valenzuela, Optimized protocol for the preparation of multi-walled carbon nanotube: polystyrene transducers for electrochemical sensing, *Instrum. Sci. Technol.*, **2021**, *49*, 327-341. [Crossref], [Google Scholar], [Publisher]

[2] A.G. Bannov, A.M. Manakhov, D.V. Shtansky. Plasma Functionalization of Multi-Walled Carbon Nanotubes for Ammonia Gas Sensors, *Materials*, **2022**, *15*, 7262. [Crossref], [Google Scholar], [Publisher]

[3] E.M. Remillard, Q. Zhang, S. Sosina, Z. Branson, T. Dasgupta, C.D. Vecitis, Electric-field alignment of aqueous multi-walled carbon nanotubes on microporous substrates, *Carbon*, **2016**, *100*, 578-589. [Crossref], [Google Scholar], [Publisher]

[4] R. Shoukat, M.I. Khan, Carbon nanotubes: a review on properties, synthesis methods and applications in micro and nanotechnology, *Micro. Technol.*, **2021**, 1-10. [Crossref], [Google Scholar], [Publisher]

[5] S. Chockalingam, A. Bisht, O.S. Panwar, A.K. Kesarwani, B.P. Singh, J. Chand, V.N. Singh, Synthesis, structural and field emission properties of multiwall carbon nanotube-graphene-like nanocarbon hybrid films grown by microwave plasma enhanced chemical vapor deposition, *Mater. Chem. Phys.*, **2015**, *156*, 38-46. [Crossref], [Google Scholar], [Publisher]

[6] A. Bisht, S. Chockalingam, O.S. Panwar, A.K. Kesarwani, B.P. Singh, V.N. Singh, Structural, field emission and ammonia gas sensing properties of multiwalled carbon nanotube-graphene like hybrid films deposited by microwave plasma enhanced chemical vapor deposition technique, *Sci. Adv. Mater.*, **2015**, *7*, 1424-1434. [Crossref], [Google Scholar], [Publisher]

[7] P. Pandey, M. Dahiya, Carbon nanotubes: Types, methods of preparation and applications, *Carbon*, **2016**, *1*, 15-21. [Google Scholar], [PDF]

[8] H. Du, X. Maimaitiyiming, Y. Luo, A. Obold. A highly sensitive ammonia gas sensor based on non-covalent functionalized single-walled carbon nanotubes with Schiff Base polyphenylene polymer, *Sens. Actuators B Chem.*, **2023**, *394*, 134426. [Crossref], [Google Scholar], [Publisher]

[9] A. Khamsavi, Y. Abdi, M.Z. Meymian, A novel two-electrode nonenzymatic electrochemical glucose sensor based on vertically aligned carbon nanotube arrays, *IEEE Sens. J.*, **2019**, *3*, 1-4. [Crossref], [Google Scholar], [Publisher]

[10] A.G. Bannov, O. Jašek, A. Manakhov, M. Márik, D. Nečas, L. Zajíčková, High-performance ammonia gas sensors based on plasma treated carbon nanostructures, *IEEE Sens. J.*, **2017**, *17*, 1964-1970. [Crossref], [Google Scholar], [Publisher]

[11] S. Kumar, V. Pavelyev, P. Mishra, N. Tripathi, A review on chemiresistive gas sensors based on carbon nanotubes: device and technology transformation, *Sens. Actuator. A. Phys.*, **2018**, *283*, 174-186. [Crossref], [Google Scholar], [Publisher]

[12] R. Aslam, C.M. Hussain, J. Aslam, Surface modified carbon nanotubes for lab on chip devices, in surface modified carbon nanotubes volume 1: fundamentals, synthesis and recent trends, *J. Am. Chem. Soc.*. **2022**, 181-193. [Crossref], [Google Scholar], [Publisher]

[13] Z. Shao, Y. Chang, B.J. Venton. Carbon microelectrodes with customized shapes for neurotransmitter detection: A review. *Anal. Chim. Acta*, **2022**, *1223*, 340165. [Crossref], [Google Scholar], [Publisher]

[14] A. Oyewemi, A.S. Abdulkareem, J.O. Tijani, M.T. Bankole, O.K. Abubakre, A.S. Afolabi, W. D. Roos. Controlled syntheses of multi-walled carbon nanotubes from bimetallic Fe–Co catalyst supported on kaolin by chemical vapour deposition method. *Arab J Sci Eng*, **2019**, *44*, 5411-5432. [Crossref], [Google Scholar], [Publisher]

[15] R. Chen, Y. Xue, X. Xu, H. Yang, T. Qiu, L. Shui, X. Wang, G. Zhou, M. Giersig, S. Pidot, J. A. Hutchison, E.M. Akinoglu. Lithography-free synthesis of periodic, vertically-aligned, multi-walled carbon nanotube arrays. *Nanotechnology*, **2021**, *33*, 065304. [Crossref], [Google Scholar], [Publisher]

[16] M.R. Baez-Gaxiola, J.A. García-Valenzuela. Optimized protocol for the preparation of multi-walled carbon nanotube: polystyrene transducers for electrochemical sensing. *Instrum. Sci. Technol.*, **2021**, *49*, 327-341. [Crossref], [Google Scholar], [Publisher]

[17] E.M. Remillard, Q. Zhang, S. Sosina, Z. Branson, T. Dasgupta, C.D. Vecitis. Electric-field alignment of aqueous multi-walled carbon nanotubes on microporous substrates. *Carbon*, **2016**, *100*, 578-589. [Crossref], [Google Scholar], [Publisher]

[18]R. Hufschmid, H. Arami, R.M. Ferguson, M. Gonzales, E. Teeman, L.N. Brush, N. D. Browning, K.M. Krishnan. Synthesis of phase-pure and monodisperse iron oxide nanoparticles by thermal decomposition. *Nanoscale*, **2015**, *7*, 11142-11154. [Crossref], [Google Scholar], [Publisher]

[19] A. Lassenberger, T.A. Grunewald, P.D.J. Van Oostrum, H. Rennhofer, H. Amenitsch, R. Zirbs, H. C. Lichtenegger, E. Reimhult. Monodisperse iron oxide nanoparticles by thermal decomposition: elucidating particle formation by second-resolved in situ small-angle X-ray scattering. *Chem. Mater.*, **2017**, *29*, 4511-4522. [Crossref], [Google Scholar], [Publisher]

[20] M. Kubo, K. Kusdianto, H. Masuda, M. Shimada. Fabrication of a metal oxide layer on a multi-walled carbon nanotube surface by in-flight coating using gas-phase deposition. *Ceram. Int.*, **2016**, *42*, 9162-9169. [Crossref], [Google Scholar], [Publisher]

[21] F. Ahmed, S. Kumar, N.M. Shaalan, O. Saber, S. Rehman, A. Aljaafari, H. Abuhimd, M. Alshahrani. Synergistic Effect of Hexagonal Boron Nitride-Coated Separators and Multi-Walled Carbon Nanotube Anodes for Thermally Stable Lithium-Ion Batteries. *Crystals*, **2022**, *12*, 125. [Crossref], [Google Scholar], [Publisher]

[22] L.T.M. Hoa. Characterization of multi-walled carbon nanotubes functionalized by a mixture of HNO3/H2SO4. *Diam. Relat. Mater*, **2018**, *89*, 43-51. [Crossref], [Google Scholar], [Pdf]

[23] M. Goyal, N. Goyal, H. Kaur, A. Gera, K. Minocha, P. Jindal. Fabrication and characterisation of low density polyethylene (LDPE)/multi walled carbon nanotubes (MWCNTs) nano-composites. *Perspect. Sci*., **2016**, *8*, 403-405. [Crossref], [Google Scholar], [Publisher]

[24] H.M. Park, G.M. Kim, S.Y. Lee, H. Jeon, S. Y. Kim, M. Kim, Y.C. Jung, B.J. Yang. Electrical resistivity reduction with pitch-based carbon fiber into multi-walled carbon nanotube (MWCNT)-embedded cement composites. *Constr*. *Build. Mater*., **2018**, *165*, 484-493. [Crossref], [Google Scholar], [Publisher]

[25] J. Yang, X. Li, C. Liu, G. Ma. Changes of structure and electrical conductivity of multi-walled carbon nanotubes film caused by 3 MeV proton irradiation. *Appl. Surf. Sci*., **2015**, *325*, 235-241. [Crossref], [Google Scholar], [Publisher]

[26] H. Ezgin, E. Demir, S. Acar, M. Özer. Investigation of temperature-dependent electrical parameters in a Schottky barrier diode with multi-walled carbon nanotube (MWCNT) interface. *Mater. Sci. Semicond. Process*., **2022**, *147*, 106672. [Crossref], [Google Scholar], [Publisher]

[27 G.V. Prasad, V. Vinothkumar, S.J. Jang, T. H. Kim. Multi-walled carbon nanotube/graphene oxide/poly (threonine) composite electrode for boosting electrochemical detection of paracetamol in biological samples. *Microchem. J*., **2023**, *184*, 108205. [Crossref], [Google Scholar], [Publisher]

[28] D. Balram, K.Y. Lian, N. Sebastian. Synthesis of a functionalized multi-walled carbon nanotube decorated ruskin michelle-like ZnO nanocomposite and its application in the development of a highly sensitive hydroquinone sensor. *Inorg. Chem. Front*., **2018**, *5*, 1950-1961. [Crossref], [Google Scholar], [Publisher]

[29] S. Yashiro, Y. Sakaida, Y. Shimamura, Y. Inoue. Evaluation of interfacial shear stress between multi-walled carbon nanotubes and epoxy based on strain distribution measurement using Raman spectroscopy. *Compos. Part A: Appl. Sci. Manuf*., **2016**, *85*, 192-198. [Crossref], [Google Scholar], [Publisher]

[30] G.H. Wu, S.Q. Liu, X.Y. Wu, X.M. Ding. Influence of MWCNTs modified by silane coupling agent KH570 on the properties and structure of MWCNTs/PLA composite film. *J. Polym. Res*., **2016**, *23*, 1-8. [Crossref], [Google Scholar], [Publisher]

[31]Y. Fan, G. Wu, F. Su, K. Li, L. Xu, X. Han, Y. Yan. Lipase oriented-immobilized on dendrimer-coated magnetic multi-walled carbon nanotubes toward catalyzing biodiesel production from waste vegetable oil. *Fuel*, **2016**, *178*, 172-178. [Crossref], [Google Scholar], [Publisher]

[32] P.A. de León-Martínez, A. Sáenz-Galindo, C. A. Ávila-Orta, A.O. Castañeda-Facio, M.L. Andrade-Guel, U. Sierra, G. Alvarado-Tenorio, J. Bernal-Martínez. Ultrasound-Assisted Surface Modification of MWCNT Using Organic Acids. *Materials*, **2020**, *14*, 72. [Crossref], [Google Scholar], [Publisher]

[33] T. Alizadeh, S. Nayeri. An enzyme-free sensing platform based on molecularly imprinted polymer/MWCNT composite for sub-micromolar-level determination of pyruvic acid as a cancer biomarker. *Anal. Bioanal. Chem*., **2020**, *412*, 657-667. [Crossref], [Google Scholar], [Publisher]

[34] D.V. Wagle, C.A. Deakyne, G.A. Baker. Quantum chemical insight into the interactions and thermodynamics present in choline chloride based deep eutectic solvents. *J. Phys. Chem. B*, **2016**, *120*, 6739-6746. [Crossref], [Google Scholar], [Publisher]

[35] C. Velez, O. Acevedo. Simulation of deep eutectic solvents: Progress to promises. Wiley Interdiscip. *Rev. Comput. Mol. Sci*., **2022**, *12*, e1598. [Crossref], [Google Scholar], [Publisher]

[36] D.K. Mishra, G. Gopakumar, G. Pugazhenthi, C.V. Siva Brahmmananda Rao, S. Nagarajan, T. Banerjee. Molecular and spectroscopic insights into a metal salt-based deep eutectic solvent: a combined quantum theory of atoms in molecules, noncovalent interaction, and density functional theory study. *J. Phys. Chem. A*., **2021**, *125*, 9680-9690. [Crossref], [Google Scholar], [Publisher]

[37] A. González de Castilla, J.P. Bittner, S. Müller, S. Jakobtorweihen, I. Smirnova. Thermodynamic and transport properties modeling of deep eutectic solvents: A review on gE-models, equations of state, and molecular dynamics. *J. Chem. Eng. Data*, **2019**, *65*, 943-967. [Crossref], [Google Scholar], [Publisher]

[38] B. B. Hansen, S. Spittle, B. Chen, D. Poe, Y. Zhang, J. M. Klein, A. Horton, L. Adhikari, T. Zelovich, B. W. Doherty, B. Gurkan, E. J. Maginn, A. Ragauskas, M. Dadmun, T. A. Zawodzinski, G. A. Baker, M. E. Tuckerman, R. F. Savinell, J. R. Sangoro. Deep eutectic solvents: A review of fundamentals and applications. *Chem. Rev*., **2020**, *121*, 1232-1285. [Crossref], [Google Scholar], [Publisher]

[39] C. Ma, A. Laaksonen, C. Liu, X. Lu, X. Ji. The peculiar effect of water on ionic liquids and deep eutectic solvents. *Chem. Soc.Rev*., **2018**, *47*, 8685-8720. [Crossref], [Google Scholar], [Publisher]

[40] M. BinSabt, M. Shaban, A. Gamal. Nanocomposite Electrode of Titanium Dioxide Nanoribbons and Multiwalled Carbon Nanotubes for Energy Storage. *Materials*, **2023**, *16*, 595. [Crossref], [Google Scholar], [Publisher]

[41] M. Shaban, A.M. Ashraf, H. AbdAllah, H. M. Abd El-Salam. Titanium dioxide nanoribbons/multi-walled carbon nanotube nanocomposite blended polyethersulfone membrane for brackish water desalination. *Desalination*, **2018**, *444*, 129-141. [Crossref], [Google Scholar], [Publisher]

[42] S. Ebrahimi, D. Souri, A. Khezripour. Strain-size features of bare ZnSe: Cu and ZnSe: Cu@ ZnS core/shell quantum dots from extensive X-ray diffraction analysis, and their photoluminescence properties. *J. Lumin*., **2022**, *244*, 118757. [Crossref], [Google Scholar], [Publisher]

[43] S.K. Sen, U.C. Barman, M.S. Manir, P. Mondal, S. Dutta, M. Paul, M A M Chowdhury, M.A. Hakim. X-ray peak profile analysis of pure and Dy-doped α-MoO3 nanobelts using Debye-Scherrer, Williamson-Hall and Halder-Wagner methods. *ANSN*, **2020**, *11*, 025004. [Crossref], [Google Scholar], [Publisher]

[44] Y. Cornaton, J.P. Djukic. Noncovalent interactions in organometallic chemistry: from cohesion to reactivity, a new chapter. *Acc. Chem. Res*., **2021**, *54*, 3828-3840. [Crossref], [Google Scholar], [Publisher]

[45] A.M. MAhArrAMov, K.T. MAhMudov. Non-covalent Interactions in the Synthesis and Design of New Compounds. **2016** [Crossref], [Google Scholar], [Publisher]

[46] P. Hobza, J. Rezac. Introduction: noncovalent interactions. *Chem. Rev*., **2016**, *116*, 4911-4912. [Crossref], [Google Scholar], [Publisher]

[47] L.C. Williams, S.M. Underwood, M.W. Klymkowsky, M.M. Cooper. Are noncovalent interactions an Achilles heel in chemistry education? A comparison of instructional approaches. *J. Chem. Edu*., **2015**, *92*, 1979-1987. [Crossref], [Google Scholar], [Publisher]

[48] K.T. Mahmudov, A.V. Gurbanov, F.I. Guseinov, M.F.C.G. da Silva. Noncovalent interactions in metal complex catalysis. *Coord. Chem. Rev*., **2019**, *387*, 32-46. [Crossref], [Google Scholar], [Publisher]

[49] F.D. Toste, M.S. Sigman, S.J. Miller. Pursuit of noncovalent interactions for strategic site-selective catalysis. *Acc. Chem. Res*., **2017**, *50*, 609-615. [Crossref], [Google Scholar], [Publisher]

[50] Y. Cornaton, J.P. Djukic. Noncovalent interactions in organometallic chemistry: from cohesion to reactivity, a new chapter. *Acc. Chem. Res*., **2021**, *54*, 3828-3840. [Crossref], [Google Scholar], [Publisher]

[51] J.C. Lewis. Beyond the second coordination sphere: engineering dirhodium

artificial metalloenzymes to enable protein control of transition metal catalysis. *Acc. Chem. Res.*, **2019**, *52*, 576-584. [Crossref], [Google Scholar], [Publisher]

[52] S. Afewerki, U. Edlund. Combined Catalysis: A Powerful Strategy for Engineering Multifunctional Sustainable Lignin-Based Materials. *ACS nano*, **2023**, *17*, 7093-7108. [Crossref], [Google Scholar], [Publisher]

[53] B.S. Bouley, F. Tang, D.Y. Bae, L.M. Mirica. C–H bond activation via concerted metalation–deprotonation at a palladium (iii) center. *Chem. Sci.*, **2023**, *14*, 3800-3808. [Crossref], [Google Scholar], [Publisher]

[54] Y. Cornaton, J.P. Djukic. Noncovalent interactions in organometallic chemistry: from cohesion to reactivity, a new chapter. *Acc. Chem. Res.*, **2021**, *54*, 3828-3840. [Crossref], [Google Scholar], [Publisher]

[55] D.Y. Yoo, I. You, S.J. Lee. Electrical and piezoresistive sensing capacities of cement paste with multi-walled carbon nanotubes. *Archiv. Civ. Mech. Eng.*, **2018**, *18*, 371-384. [Crossref], [Google Scholar], [Publisher]

[56] B. Şimşek, T. Uygunoğlu, Ö. F. Dilmaç. Comparative evaluation of the effectiveness of PTFE nanoparticles on cement pastes properties with multi-wall carbon nanotubes, graphene oxide and silver nanoparticles. *Constr. Build. Mater.*, **2022**, *319*, 126077. [Crossref], [Google Scholar], [Publisher]

[57] M. Karakouzian, V. Farhangi, M.R. Farani, A. Joshaghani, M. Zadehmohamad, M. Ahmadzadeh. Mechanical characteristics of cement paste in the presence of carbon nanotubes and silica oxide nanoparticles: An experimental study. *Materials*, **2021**, *14*, 1347. [Crossref], [Google Scholar], [Publisher]

[58] S. Żarska, D. Kulawik, J. Drabowicz, W. Ciesielski. A review of procedures of purification and chemical modification of carbon nanotubes with bromine. *Fuller., Nanotub. Carbon Nanostructures*, **2017**, *25*, 563-569. [Crossref], [Google Scholar], [Publisher]

[59] S. Zdanowska, M. Pyzalska, J. Drabowicz, D. Kulawik, V. Pavlyuk, T. Girek, W. Ciesielski. Carbon nanotubes functionalized by salts containing stereogenic heteroatoms as electrodes in their battery cells. *Pol. J. Chem. Technol.*, **2016**, *18*, 22-26. [Crossref], [Google Scholar], [Publisher]

[60] J. Drabowicz, D. Krasowska, W. Ciesielski, D. Kulawik, M. Pyzalska, S. Zdanowska, P. Pokora-Sobczak, J. Chrzanowski, T. Makowski. Carbon nanotubes functionalized with sulfur, selenium, or phosphorus or substituents containing these elements. *Phosphorus, Sulfur, Silicon Relat Elem.*, **2016**, *191*, 541-547. [Crossref], [Google Scholar], [Publisher]

[61] I. Abdulazeez, B. Salhi, A.M. Elsharif, M. S. Ahmad, N. Baig, M.M. Abdelnaby. Hemin-Modified Multi-Walled Carbon Nanotube-Incorporated PVDF Membranes: Computational and Experimental Studies on Oil–Water Emulsion Separations. *Molecules*, **2023**, *28*, 391. [Crossref], [Google Scholar], [Publisher]

[62] C.L. Brito, E.I. Ferreira, M.A. La-Scalea. Application of multi-walled carbon nanotubes functionalized with hemin to evaluate the electrochemical behavior of nitrofurazone in aqueous media. *Electrochim. Acta.*, **2023**, *459*, 142486. [Crossref], [Google Scholar], [Publisher]

[63] R. Parmar, J. Rezvani, M. Amati, L. Gregoratti, D.B.D.F. Neto, J.M. Rosolen, R. Gunnella. Effect of Carbon Nanotubes on the Na+ Intercalation Capacity of Binder Free Mn2V2O7-CNTs Electrode: A Structural Investigation. *Materials*, **2023**, *16*, 2069. [Crossref], [Google Scholar], [Publisher]

[64] D. B. D Freitas Neto. Eletrodos binder-free para baterias e supercapacitores de lítio baseados em nanocompósitos de carbono e óxidos metálicos: uma avaliação de viabilidade técnica (Doctoral dissertation, Universidade de São Paulo). **2023**. [Crossref], [Google Scholar], [Publisher]

[65] A.J. Fernández-Ropero, D. Saurel, B. Acebedo, T. Rojo, M. Casas-Cabanas. Electrochemical characterization of NaFePO4 as positive electrode in aqueous sodium-ion

batteries. *J. Power Sources*, **2015**, 291, 40-45. [Crossref], [Google Scholar], [Publisher]
[66] H. Fawzy, M.S. Ghareeb, H. Mosaad, Implication of plasma miR 122 and miR 151-3p levels in diagnosis and prognosis of acute coronary syndrome patients, *J. Med. Chem. Sci.*, **2023**, In Press. [Crossref], [Pdf], [Publisher]
[67] P. Pandey, M. Dahiya. Carbon nanotubes: Types, methods of preparation and applications, *Carbon*, **2016**, *1*, 15-21. [Google Scholar], [Pdf]
[68] F. Ahmadzade, S. Safa, P. Balashabady. Growth of vertically aligned carbon nanotubes by DCPECVD system and the effects of C2H2 concentration and plasma current on the growth behavior of CNTs. *Arab. J. Sci. Eng.*, **2011**, *36*, 97-103. [Crossref], [Google Scholar], [Publisher]
[69] I.J. Teng, K.L. Chen, H.L. Hsu, S.R. Jian, L. C. Wang, J. H. Chen, C.T. Kuo. Highly graphitized laterally interconnected SWCNT network synthesis via a sandwich-grown method. *J. Phys. D: Appl. Phys.*, **2011**, *44*, 145401. [Crossref], [Google Scholar], [Publisher]
[70] S.A. Etghani, E. Ansari, S. Mohajerzadeh. Evolution of large area TiS_2-TiO_2 heterostructures and S-doped TiO_2 nano-sheets on titanium foils. *Sci. Rep.*, **2019**, *9*, 17943. [Crossref], [Google Scholar], [Publisher]

How to cite this article: Rahadian Zainul, Matlal Fajri Alif, Ani Mulyasuryani. Advancements in plasma-enhanced chemical vapor deposition of a multi-walled carbon nanotubes on Si/SiO_2 substrates: A comprehensive review. *Journal of Medicinal and Pharmaceutical Chemistry Research*, 2023, 5(11), 1013-1033. **Link:** http://jmpcr.samipubco.com/article_180906.html

Copyright © 2023 by SPC (Sami Publishing Company) + is an open access article distributed under the Creative Commons Attribution License(CC BY) license (https://creativecommons.org/licenses/by/4.0/), which permits unrestricted use, distribution, and reproduction in any medium, provided the original work is properly cited.